

Hole Transfer in a C-Shaped Molecule: Conformational Freedom versus Solvent-Mediated Coupling

Jocelyn M. Nadeau,^{†,§} Min Liu,[‡] David H. Waldeck,^{*,‡} and Matthew B. Zimmt^{*,†}

Contribution from the Department of Chemistry, Brown University, Providence, Rhode Island 02912, and Department of Chemistry, University of Pittsburgh, Pittsburgh, Pennsylvania 15260

Received July 15, 2003; E-mail: Dave@Pitt.edu; Matthew_Zimmt@Brown.Edu

Abstract: The electronic coupling matrix elements attending the charge separation reactions of a C-shaped molecule containing an excited pyrene as the electron acceptor and a dimethylaniline as the donor are determined in aromatic, ether, and ester solvents. Band shape analyses of the charge-transfer emission spectra ($CT \rightarrow S_0$) provide values of the reaction free energy, the solvent reorganization energy, and the vibrational reorganization energy in each solvent. The free energy for charge separation in benzene and toluene solvents is independently determined from the excited state equilibrium established between the locally excited pyrene S_1 state and the charge-transfer state. Analyses of the charge separation kinetics using the spectroscopically determined reorganization energies and reaction free energies indicate that the electronic coupling is solvent independent, despite the presence of a cleft between the donor and acceptor. Hence, solvent molecules are not involved in the coupling pathway. The orientations of the donor and acceptor units, relative to the spacer, are not rigidly constrained, and their torsional motions decrease solvent access to the cleft. Generalized Mulliken–Hush calculations show that rotation of the pyrene group about the bond connecting it to the spacer greatly modulates the magnitude of through-space coupling between the S_1 and CT states. The relationship between the torsional dynamics and the electron-transfer dynamics is discussed.

I. Introduction

The great progress in understanding unimolecular electron-transfer processes during the past two decades has occurred by combining experiments and theoretical calculations on well-defined donor–spacer–acceptor molecules.¹ In these studies, the electron-transfer rate constant is described by a Golden Rule expression which treats nuclear and electronic degrees of freedom as independent quantities.² This rate formulation is appropriate when the donor–acceptor electronic coupling (which is a measure of these groups' quantum mechanical mixing) is small and the same every time the transition state is accessed. This criterion (the Condon approximation) is best satisfied in conformationally restricted systems, such as “rigid”, linear donor–bridge–acceptor molecules. The dependence of electronic coupling magnitude on bridge structure in a variety of

“rigid” systems has been investigated and is well understood.³ In contrast to such systems, the C-shaped molecule studied here has two potential sources of nuclear coordinate-dependent electronic coupling: (i) a direct, through-space interaction that is modulated by the conformational freedom of the donor and acceptor groups and (ii) an indirect, solvent-mediated interaction that is modulated by a solvent molecule's placement in the cleft that lies between the donor and acceptor. The influence of these nuclear coordinates on the overall electronic coupling and on the electron-transfer process is explored in this investigation.

The dynamical consequences of nuclear coordinate-dependent electronic coupling have been addressed in a number of limiting cases. When interconversion rates between a predominant system conformation and a number of highly reactive conformations are slow, the experimental transfer rate constant reflects conformational dynamics more than intrinsic electron-transfer rate constants; that is, the system is conformationally gated.⁴ Additional kinetic complexity arises in systems when intercon-

[†] Brown University.

[‡] University of Pittsburgh.

[§] Present address: Department of Chemistry, Massachusetts Institute of Technology, Cambridge, MA 02139.

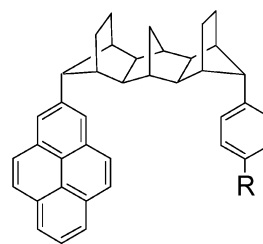
(1) (a) Closs, G. L.; Miller, J. R. *Science* **1988**, *240*, 440. (b) Barbara, P. F.; Meyer, T. J.; Ratner, M. A. *J. Phys. Chem.* **1996**, *100*, 13148. (c) Lewis, F. D.; Letsinger, R. L.; Wasielewski, M. R. *Acc. Chem. Res.* **2001**, *34*, 159. (d) Davis, W. B.; Ratner, M. A.; Wasielewski, M. R. *Chem. Phys.* **2002**, *281*, 333. (e) Jordan, K. D.; Paddon-Row, M. N. *Chem. Rev.* **1992**, *92*, 395. (f) Newton, M. D. *Chem. Rev.* **1991**, *91*, 767.
(2) (a) Reimers, J. R.; Hush, N. S. *Chem. Phys.* **1989**, *134*, 323. (b) Todd, M. D.; Nitzan, A.; Ratner, M. A. *J. Phys. Chem.* **1993**, *97*, 29. (c) Rips, I.; Jortner, J. *Jerusalem Symp. Quantum Chem. Biochem.* **1990**, *22*, 293–9. (d) Baym, G. *Lectures on Quantum Mechanics*; Benjamin-Cummings: London, 1981; pp 248–58.

(3) (a) Oevering, H.; Paddon-Row, M. N.; Heppener, M.; Oliver, A. M.; Cotsaris, E.; Verhoeven, J. W.; Hush, N. S. *J. Am. Chem. Soc.* **1987**, *109*, 3258. (b) Winkler, J. R.; Gray, H. B. *J. Biol. Inorg. Chem.* **1997**, *2*, 399. (c) Helms, A.; Heiler, D.; McLendon, G. *J. Am. Chem. Soc.* **1991**, *113*, 4325. (d) Shin, Y.-G. K.; Newton, M. D.; Isied, S. S. *J. Am. Chem. Soc.* **2003**, *125*, 3722. (e) Kang, Y. K.; Rubtsov, I. V.; Iovine, P. M.; Chen, J.; Therien, M. J. *J. Am. Chem. Soc.* **2002**, *124*, 8275.
(4) (a) Cartling, Bo. *J. Chem. Phys.* **1985**, *83*, 5231. (b) Blair, D. F.; Gelles, J.; Chan, S. I. *Biophys. J.* **1986**, *50*, 713. (c) Hoffman, B. M.; Ratner, M. A. *J. Am. Chem. Soc.* **1987**, *109*, 6237. (d) McLendon, G.; Pardue, K.; Bak, P. *J. Am. Chem. Soc.* **1987**, *109*, 7540.

version rates among multiple reactive conformations are comparable to the transfer rate constants of the individual conformations. A different category of complexity arises if a set of nuclear coordinates influences the barrier to electron transfer (i.e., the nuclear Franck–Condon factors) and also strongly modulates the donor–acceptor electronic coupling. This produces an explicit nuclear dependence of the coupling matrix element, which violates the Condon approximation and may invalidate use of the Golden Rule rate expression. Systems that may fall into this category include protein electron transfers,⁵ symmetry forbidden but vibronically allowed electron transfers,⁶ and solvent-mediated electron transfers.⁷ In the latter systems, different placements of solvent molecules generate different values of the donor–acceptor coupling matrix element, thus altering the electron tunneling probability, and at the same time contribute to the activation barrier through solvation and reorganization effects.

During the past few years, we have analyzed electron-transfer dynamics from a number of systems in which coupling is primarily solvent mediated. These investigations employ rigid C-shaped structures with a solvent-accessible cleft directly between the donor and acceptor groups. The rigidity guarantees that each molecule populates only one conformation. The length and topology of the spacers, in conjunction with the attachment geometries of the donor and acceptor, were designed to reduce through-bond coupling magnitudes so that solvent-mediated coupling dominates. In these systems, solvent molecules within the cleft constitute the electron tunneling pathway between the donor and acceptor group. Striking evidence for the solvent's participation in the electron tunneling pathway comes from the strong correlation between the experimentally derived electronic coupling magnitude and the solvent's LUMO energy.⁸ Because the electron-transfer reaction within the C-shaped molecule is initiated by photoexcitation of the donor, the transferring electron originates in the donor LUMO. The energetic proximity of vacant solvent orbitals to the LUMO of the excited donor provides a rationale for the observed correlations. Solvent molecules with a lower energy LUMO enhance the excited donor to acceptor coupling because they provide lower energy excited configurations (resonance structures), such as D^+S^-A , that more effectively mix into the donor excited state and, simultaneously, increase the acceptor's proximity to the transferring electron.⁹ This explanation suggests that a C-shaped molecule employing an electronically excited acceptor might display solvent-mediated coupling magnitudes that correlate with solvent HOMO energy; that is, energetic proximity of solvent

Scheme 1

1. R = NMe₂

2. R = H

valence orbitals to the transferring hole in the HOMO of an excited acceptor should enhance electron tunneling from D to A*.

This manuscript analyzes the electron-transfer kinetics and charge-transfer emission spectra from a C-shaped molecule containing an excited acceptor and a ground state donor. Molecule **1** (Scheme 1) has a 2'-pyrenyl acceptor (A) and a 4'-N,N-dimethylaniliny donor (D) that are connected by single bonds to the terminal, CH₂ bridges of a tetradecahydro-1,4:5,8:9,10-trimethanoanthracene spacer. Eight σ bonds separate the acceptor and donor groups. In the molecule's lowest energy conformation, the pyrene and dimethylaniline groups lie in roughly parallel planes displaced by 6.7 Å. Molecular mechanics calculations indicate that the cleft defined by the donor, spacer, and acceptor is just large enough to accommodate aromatic or other nearly planar solvent molecules. The gas phase, vertical ionization potential of dimethylaniline is ~ 7.4 eV.¹⁰ The gas phase, vertical ionization potentials of the solvents employed in this investigation range from 8.4 eV (anisole) to 10.4 eV (ethyl acetate). The energy of a virtual $(A^-)-(solvent^+)-D$ superexchange^{9a,b} configuration changes substantially across this set of solvents, as should its mixing with the acceptor excited state.⁸ If donor–acceptor coupling in **1** is predominantly solvent mediated, the experimentally determined coupling value ought to decrease as the energy of the virtual^{9a} $A^-(solvent^+)-D$ configuration increases, that is, from anisole to ethyl acetate. In contrast to this prediction, the experimentally determined coupling magnitudes are solvent independent, exhibiting no correlation with solvent ionization potential (HOMO level) or solvent electron affinity (LUMO level). This is evidence against the involvement of solvent in the electron tunneling pathway. Surprisingly, calculations reveal negligible electronic coupling in the lowest energy conformation of molecule **1**, indicating that through-space and through-bond tunneling pathways are inactive. Instead, the calculations predict large donor–acceptor* electronic coupling in conformations formed by twisting the pyrene or the dimethylaniline about the σ bonds connecting these groups to the spacer. Taken together, the experiments and calculations indicate that donor–acceptor electronic coupling

- (5) (a) Beratan, D. N.; Hopfield, J. J. *J. Chem. Phys.* **1984**, *81*, 5753. (b) Skourtis, S. S.; Archontis, G.; Xie, Q. *J. Chem. Phys.* **2001**, *115*, 9444. (c) Skourtis, S. S. *Chem. Phys. Lett.* **2003**, *372*, 224. (d) Medvedev, E. S.; Stuchebrukhov, A. A. *J. Chem. Phys.* **1997**, *107*, 3821. (e) Ungar, L. W.; Newton, M. D.; Voth, G. A. *J. Phys. Chem. B* **1999**, *103*, 7367. (f) Mikkelsen, K. V.; Ulstrup, J.; Zakarayya, M. G. *J. Am. Chem. Soc.* **1989**, *111*, 1315. Related treatments not specific to proteins include: (g) Tang, J. J. *J. Chem. Phys.* **1993**, *98*, 6263. (h) Bixon, M.; Jortner, J. *Russ. J. Electrochem.* **2003**, *39*, 3.
- (6) (a) Reimers, J. R.; Hush, N. S. *Chem. Phys.* **1990**, *146*, 105. (b) Jones, G. A.; Paddon-Row, M. N.; Carpenter, B. K.; Piotrowiak, P. *J. Phys. Chem. A* **2002**, *106*, 5011.
- (7) (a) Lawson, J. M.; Paddon-Row, M. N.; Schuddeboom, W.; Warman, J. M.; Clayton, A. H. A.; Ghiggino, K. P. *J. Phys. Chem.* **1993**, *97*, 13099. (b) Kumar, K.; Lin, Z.; Waldeck, D. H.; Zimmt, M. B. *J. Am. Chem. Soc.* **1996**, *118*, 243. (c) Read, I.; Napper, A.; Kaplan, R.; Zimmt, M. B.; Waldeck, D. H. *J. Am. Chem. Soc.* **1999**, *121*, 10976. (d) Napper, A. M.; Read, I.; Waldeck, D. H.; Kaplan, R. W.; Zimmt, M. B. *J. Phys. Chem. A* **2002**, *106*, 4784. (e) Milischuk, A.; Matyushov, D. V. *J. Chem. Phys.* **2003**, *118*, 5596.
- (8) Zimmt, M. B.; Waldeck, D. A. *J. Phys. Chem. A* **2003**, *107*, 3580.

- (9) The energy of D^+S^-A electronic configurations are too far above the D^*SA configuration to allow significant thermal population. D^+S^-A configurations act as "virtual" states that enhance D^*A coupling via superexchange. See: (a) McConnell, H. M. *J. Chem. Phys.* **1961**, *35*, 508. (b) Liang, C.; Newton, M. D. *J. Phys. Chem.* **1993**, *97*, 3199.
- (10) (a) Kobayashi, T.; Nagakura, S. *Bull. Chem. Soc. Jpn.* **1974**, *47*, 2563. (b) Baker, A. D.; May, D. P.; Turner, D. W. *J. Chem. Soc. B* **1968**, 22. The adiabatic IP is 6.95 eV according to NIST and Mautner(Meot-Ner), M.; Nelsen, S. F.; Willi, M. R.; Frigo, T. B. *J. Am. Chem. Soc.* **1984**, *106*, 7384.

in **1** is strongly modulated by the conformational degrees of freedom of the molecule.

II. Experimental Section

The preparation of **1** and its acceptor only analogue **2** are reported elsewhere.¹¹ Samples used for steady-state spectroscopy had optical densities of 0.05–0.15 at the excitation wavelength (331 nm) in freshly dried and distilled solvents. Spectra were recorded on a SPEX F111X1 fluorimeter using 0.1 mm slits and were corrected for the detection system response. Samples for nanosecond time-resolved fluorescence spectroscopy (λ_{exc} 331 nm) and picosecond time-resolved photon counting (λ_{exc} 321 nm) were freeze–pump–thaw degassed a minimum of four cycles. Samples investigated at temperatures above 25 °C were back-filled with high purity argon to prevent solvent distillation. The apparatus for both time-resolved fluorescence methods was previously described.¹² Fluorescence decays of the excited pyrene were recorded at 380 nm to eliminate contributions from the charge-transfer (CT) emission band. Fluorescence decays of the CT band were detected at wavelengths longer than 490 nm. Fluorescence decays were fit by iterative convolution of a mono-, bi-, or triexponential expression with an instrument response function obtained from a BaSO₄–glycerol colloid. Fits to a triexponential expression were realized by adjusting three amplitudes and two decay rate constants. The slowest decay rate constant was independently determined from a single-exponential fit of the final 100 ns of the photon counting data or from a 500 ns data set obtained with the nanosecond apparatus.

Samples of compound **1** contained trace amounts of an unidentified impurity and of a pyrene–spacer molecule that lacked an active donor group. HPLC purification reduced but did not eliminate these impurities from the sample. The emission spectrum of the unidentified impurity overlapped significantly with that of pyrene; however, its decay rate constant, which varied with solvent between 0.2 and 0.5 ns⁻¹, was considerably slower than the charge separation rate constants for **1** and much faster than the decay rate constants of the CT state. The impurity's presence necessitated a triexponential analysis of the fluorescence decay, but otherwise provided little interference in the kinetic analyses or in the analyses of charge-transfer emission line shapes. The pyrene–spacer impurity contributed 3.3% of the pyrene fluorescence decay amplitude detected at 380 nm. This value was determined in polar solvents, where the S₁ → CT transition is irreversible. The contribution of this impurity was removed prior to determination of the charge separation free energy, $\Delta_r G(S_1 \rightarrow \text{CT})$, from the ratio of the fast and slow pyrene decay amplitudes.⁸

III. Results and Discussion

A. Emission Spectroscopy. The steady-state emission spectrum of **1** exhibits structured, pyrene-like peaks between 370 and 470 nm and a broad, featureless band that extends to wavelengths greater than 600 nm (Figure 1). The latter emission is obscured partially by the red edge of the pyrene-like emission. The overall intensity of the structured region varies with solvent, but the positions of the peaks remain constant at 375, 386, and 394 nm. The structured emission from **1** is assigned as fluorescence from the lowest excited singlet state (S₁, LE) of the pyrene acceptor on the basis of its similarity to the spectrum from the pyrene–spacer analogue, **2**. The intensity and position of the broad featureless emission is strongly solvent dependent. The large red shift of this band with increasing solvent polarity identifies it as a charge-transfer (CT → S₀) emission.

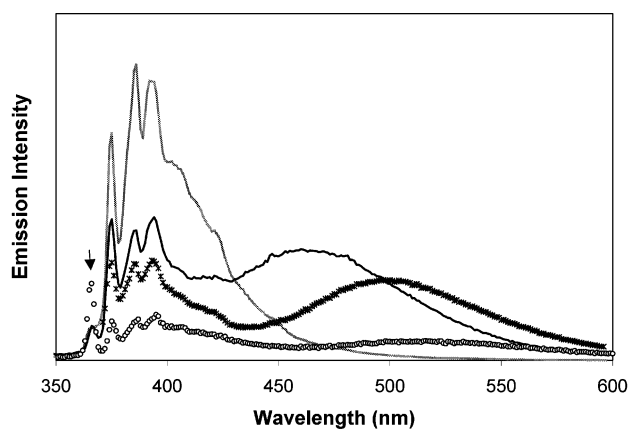


Figure 1. Steady-state fluorescence spectra from **1** in cyclohexane (gray line, intensity $\times 0.4$), benzene (black line), anisole (\times), tetrahydrofuran (\circ , intensity $\times 3.0$). The arrow points to Raman peaks (C–H) from the solvent.

Table 1. CT Emission Maxima (ν_{max}) of **1** in Dipolar Solvents at 295 K^a and Solvent Polarity Parameters, n , ϵ_s , and Δf , for Each Solvent^{b,c}

solvent	n	ϵ_s	Δf	experimental ν_{max} (cm ⁻¹)
<i>n</i> -butyl ether	1.40	3.1	0.194	21 500
<i>n</i> -propyl ether	1.38	3.4	0.214	21 200
isopropyl ether	1.37	3.9	0.238	20 800
ethyl ether	1.35	4.3	0.255	20 300
<i>n</i> -butyl propionate	1.40	4.83	0.261	19 300
<i>n</i> -butyl acetate	1.39	5.1	0.269	19 200
<i>n</i> -propyl acetate	1.38	5.5	0.281	19 000
ethyl acetate	1.37	6.0	0.292	18 700
THF	1.41	7.5	0.307	18 300

^a An instrument correction factor for the monochromator and detector response was applied to each spectrum. ^b n_D values were obtained from the Aldrich Handbook of Fine Chemicals and Laboratory Equipment, 2001–2002. ^c ϵ_s values were obtained from either: (a) Kaplan, R.; Napper, M.; Waldeck, D. H.; Zimmt, M. B. *J. Phys. Chem. A* **2002**, *106*, 1917–1925 or (b) Madelung, O. *Landolt-Börnstein Numerical Data and Functional Relationships in Science and Technology, New Series IV*; Springer-Verlag: New York, 1991; Vol. 6.

The solvatochromic shift of a CT band can be analyzed using the Lippert–Mataga relationship,^{13,14}

$$\nu_{\text{max}} = \left[\frac{-2\mu_{\text{dip}}^2}{hca^3} \right] \left[\frac{\epsilon - 1}{2\epsilon + 1} - \frac{n^2 - 1}{4n^2 + 2} \right] + \nu_{\text{max}}^0 \quad (1)$$

where ν_{max} is the CT emission maximum in a given solvent (expressed in cm⁻¹), ν_{max}^0 is the CT emission maximum for $\Delta f = 0$ (where $\Delta f = [(\epsilon - 1)/(2\epsilon + 1)] - [(n^2 - 1)/(4n^2 + 2)]$), a is the effective spherical radius of the cavity that the donor–spacer–acceptor molecule occupies in the solvent, μ_{dip} is the CT state dipole moment, ϵ is the solvent dielectric constant, and n is the refractive index of the solvent. This form of eq 1 is appropriate because the ground-state dipole moment of **1** is small (<1.5 D). CT spectra and emission maxima were determined in ether and ester solvents (Table 1). The data points (Figure 2) deviate somewhat from a straight line, with the values in acyclic ethers somewhat offset from those in the ester solvents. The slope obtained from a linear fit to the data is $-30\,560\text{ cm}^{-1}$ and yields $\mu_{\text{dip}}(D) = (3.03 \times a^3)^{1/2}$. Assuming a cavity radius of 6 or 7 Å produces a charge-separated state dipole moment of 25.6 or 32.3 D, respectively.¹⁵ These values correspond to transfer of a full electron over a distance of 5.3

(11) Nadeau, J. M. Ph.D. Thesis, Brown University, 2003.

(12) (a) Zeglinski, D. M.; Waldeck, D. H. *J. Phys. Chem.* **1988**, *92*, 692. (b) Zeng, Y.; Zimmt, M. B. *J. Phys. Chem.* **1992**, *96*, 8395.

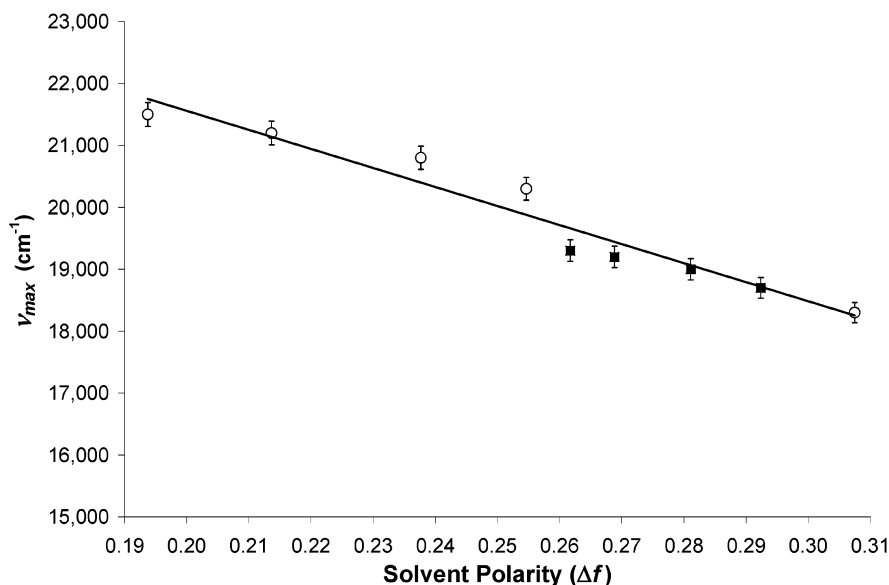


Figure 2. Lippert–Mataga plot for the CT emission band of **1** (see eq 1). Ether solvents are indicated by ○. Ester solvents are indicated with ■.

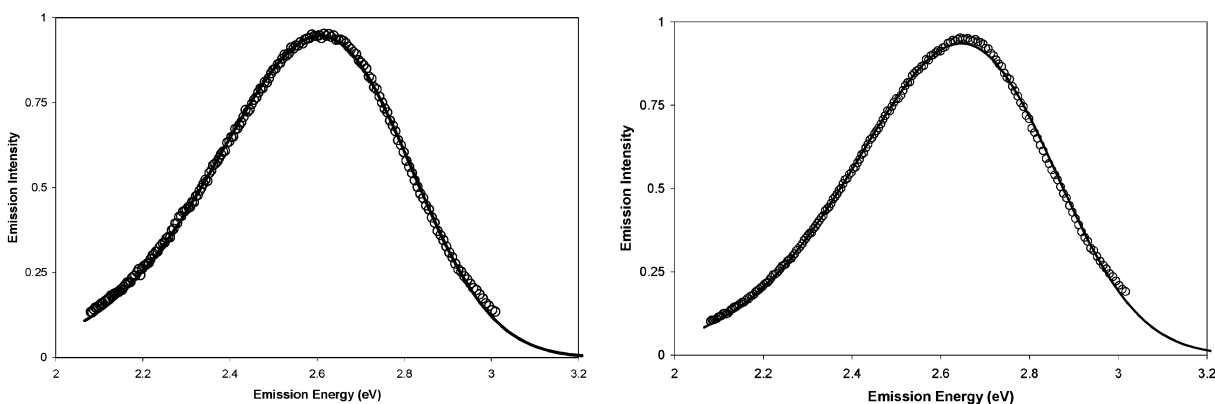


Figure 3. Experimental (○) and calculated (lines) charge-transfer emission spectra from **1** in benzene (left) and toluene (right). The spectra were calculated using $\lambda_V = 0.15$ eV, $\hbar\omega = 0.20$ eV, and $\Delta_r G(\text{CT} \rightarrow S_0) = -3.22$ eV (benzene) and -3.28 eV (toluene). Fitting yielded $\lambda_S = 0.54$ eV (benzene) and 0.56 eV in toluene.

and 6.7 Å, which is consistent with the ground state, donor–acceptor separation. The spectral analysis is too crude to determine whether charge separation induces a significant reduction of the donor–acceptor separation in **1**.

B. Electron-Transfer Thermodynamics and Reorganization Parameters. The charge recombination driving force, $\Delta_r G(\text{CT} \rightarrow S_0)$, for **1** dissolved in weakly and moderately polar solvents may be estimated through simulation of the CT emission line shape.^{16,17} Such fits provide estimates of $\Delta_r G(\text{CT} \rightarrow S_0)$ and other electron-transfer parameters included in the semiclassical model: λ_S , the solvent (low frequency) reorganization energy; λ_V , the vibrational (high frequency) reorganiza-

tion energy; and $\hbar\omega$, the average mode spacing associated with the high frequency reorganization. Many combinations of the four parameters accurately reproduce the experimental line shapes. Fortunately, **1** exhibits $\text{LE} \rightleftharpoons \text{CT}$ equilibrium in weakly polar solvents, and analysis of the kinetic data (vide infra) provides an independent value of the charge separation free energy, $\Delta_r G(S_1 \rightarrow \text{CT})$, in benzene (-0.11 eV) and toluene (-0.05 eV). These free energies were used to constrain fits to the CT spectra so as to obtain more accurate reorganization parameters.

The CT line shape analysis for **1** in benzene and toluene was constrained by setting $\Delta_r G(\text{CT} \rightarrow S_0) = -\Delta_r G(S_1 \rightarrow \text{CT}) - 3.33$ eV, where 3.33 eV is the pyrene excited state energy. The CT emission spectra from these two solvents were fit simultaneously with a single λ_V parameter for both solvents, a separate λ_S parameter for each solvent, and a single fixed value of $\hbar\omega$.¹⁸ The procedure was repeated with $\hbar\omega$ fixed to values between 0.12 and 0.22 eV in steps of 0.02 eV. The best fits were obtained with $\hbar\omega$ between 0.18 and 0.22 eV (Figure 3). The analysis yielded five ($\hbar\omega$, λ_V) pairs correlated to one of five values of

- (13) (a) Mataga, N.; Kaifu, Y.; Koizumi, M. *Bull. Chem. Soc. Jpn.* **1955**, *28*, 690–691. (b) Mataga, N.; Kaifu, Y.; Koizumi, M. *Bull. Chem. Soc. Jpn.* **1956**, *29*, 465–470.
- (14) (a) Lippert, E. *Z. Naturforsch., A* **1955**, *10a*, 541. (b) Lippert, E.; Schneider, F. *Ber. Bunsen-Ges.* **1970**, *74*, 624. (c) Lippert, E. In *Organic Molecular Photophysics*; Birks, J. B., Ed.; John Wiley and Sons: New York, 1975; Vol. 2, pp 18–19.
- (15) A CPK model of molecule **1** overlaps substantially with a CPK model of the 7 Å cleft, C-shaped molecule, **3**, previously studied (see Scheme 5).⁸ A 7.5 Å cavity radius accurately reproduced the experimental free energy data **3**. Thus, a cavity radius of 6–7 Å is reasonable for **1**.
- (16) Electron transfer from dimethylaniline to excited pyrene is more than 0.5 eV exoergic in nitrile solvents: Finckh, P.; Heitele, H.; Volk, M. Michel-Beyerle, M. E. *J. Phys. Chem.* **1988**, *92*, 6584.

- (17) (a) Marcus, R. A. *J. Phys. Chem.* **1989**, *93*, 3078. (b) Gould, I. R.; Young, R. H.; Moody, R. E.; Farid, S. *J. Phys. Chem.* **1991**, *95*, 2068.

Table 2. Charge Recombination Free Energy and Solvent Reorganization Energy Determined from the CT Emission Analyses and from a Continuum Solvation Model^a

solvent	ϵ (ϵ_{EFF}^b)	CT FC _{max} eV	$\Delta_r G(\text{CT} \rightarrow S_0)$ (line shape) eV ^c	$\Delta_r G(\text{CT} \rightarrow S_0)$ (cont.) eV ^e	λ_S (line shape) eV ^c	λ_S (cont.) ^f eV
benzene	2.3 (4.4)	-2.57	-3.22 ± 0.00^d	-3.61 (-3.18)	0.54 ± 0.02	0.22
toluene	2.4 (3.6)	-2.65	-3.28 ± 0.00^d	-3.59 (-3.23)	0.56 ± 0.02	0.18
anisole	4.3 (6.4)	-2.38	-3.10 ± 0.01	-3.40 (-3.09)	0.60 ± 0.02	0.30
ethyl ether	4.3	-2.52	-3.24 ± 0.01	-3.35	0.61 ± 0.02	0.32
butyl acetate	5.1	-2.36	-3.17 ± 0.01	-3.14	0.70 ± 0.02	0.33
chlorobenzene	5.7 (5.7)	-2.45	-3.03 ± 0.01	-3.34 (-3.34)	0.46 ± 0.02	0.28
ethyl acetate	6.0	-2.30	-3.12 ± 0.01	-3.10	0.75 ± 0.02	0.38
THF	7.5	-2.26	-3.09 ± 0.01	-3.06	0.72 ± 0.03	0.39

^a Mean value of $\hbar\omega = 0.20$ eV; mean value of $\lambda_V = 0.15$ eV. ^b See text for ϵ_{EFF} definition. ^c Errors represent one standard deviation for the five ($\hbar\omega$, λ_V) pairs. ^d Value not varied. ^e Continuum value calculated using eq 2; values in parentheses calculated using ϵ_{EFF} . ^f Continuum values calculated using eq 3 and ϵ for the nonaromatic solvents or ϵ_{EFF} for the aromatic solvents.

λ_S for benzene and for toluene. In general, larger assumed values of $\hbar\omega$ produced smaller λ_V and larger λ_S values. Line shape analyses for **1** in the remaining solvents employed the five ($\hbar\omega$, λ_V) pairs and generated five corresponding pairs of ($\Delta_r G(\text{CT} \rightarrow S_0)$, λ_S) for each solvent. Table 2 lists mean values and the range of values, as an error, for $\Delta_r G(\text{CT} \rightarrow S_0)$ and λ_S in the eight solvents. The solvent dependence of $\Delta_r G(\text{CT} \rightarrow S_0)$ determined via line shape analysis for the nonaromatic solvents (Table 2) is in reasonable agreement (within 0.1 eV) with predictions of a continuum solvation model (eq 2) using the slope of the Lippert–Mataga analysis (μ^2/a^3) and $\Delta_r G(\text{CT} \rightarrow S_0)_{\text{VAC}} = -3.83$ eV.

$$\Delta_r G(\text{CT} \rightarrow S_0) (\text{cont.}) = \Delta_r G(\text{CT} \rightarrow S_0)_{\text{VAC}} + \frac{\mu^2 (\epsilon - 1)}{a^3 (2\epsilon + 1)} \quad (2)$$

By contrast, the experimental values of $\Delta_r G(\text{CT} \rightarrow S_0)$ in the aromatic solvents are 0.3–0.4 eV less exoergic than the continuum predictions, indicating that these solvents stabilize the charge-transfer state to a greater extent than predicted by their static dielectric constants. This additional solvation arises from the aromatic solvents' large quadrupole moments.¹⁹ In the case of chlorobenzene, other factors may be involved (vide infra). Generally, the energy of a CT emission band maximum (Franck–Condon maximum¹⁸) can be approximated as $h\nu_{\text{FC-max}} \approx -\Delta_r G(\text{CT} \rightarrow S_0) - \lambda_S - \lambda_V$.²⁰ For each solvent in Table 2, $-\Delta_r G(\text{CT} \rightarrow S_0) - \lambda_S$ determined from the fit parameters is 0.1 eV larger than $h\nu_{\text{FC-max}}$.¹⁸ This suggests an approximate value of 0.1 eV for λ_V , in agreement with the value used in the fitting procedure (vide infra).

Independent estimates of vibrational reorganization energies are available from ionization energies and from theory. The difference between the vertical and adiabatic ionization potentials for aniline, ~ 0.33 eV, and for *N,N*-dimethylaniline, 0.2–

0.45 eV, indicate significant vibrational reorganization upon oxidation of aromatic amine donors.²¹ AM1 calculations predict vibrational reorganization energies, λ_V , for pyrene reduction and dimethylaniline oxidation of 0.13 and 0.23 eV, respectively. The nitrogen of dimethylaniline is pyramidal in the neutral structure and planar in the equilibrated radical cation geometry. Vibrational frequencies related to this motion are low (< 200 cm⁻¹)²² and can be treated as a low frequency (solvent) contribution in a single quantized mode model.²³ The calculated λ_V for dimethylaniline is only 0.06 eV if the dimethylamino group's improper torsion angle is constrained to the value for the neutral structure. Combined with the pyrene reorganization, this yields a total, calculated high-frequency reorganization energy of 0.19 eV, in reasonable agreement with the average value, 0.15 eV, derived from CT line shape analysis for **1** in benzene and toluene. This internal reorganization energy is associated with the planar aromatic groups, whose C=C vibrations lie near 1600 cm⁻¹. The remaining 0.17 eV of the AM1 calculated internal reorganization energy for dimethylaniline is coupled to the low frequency, pyramidalization coordinate of the dimethylamino group.

The line shape derived estimates of λ_S increase with increasing solvent dielectric constant, with the notable exception of chlorobenzene (Table 2). Overall, the values are somewhat large for the moderately polar solvents used here. The slope of the Lippert–Mataga analysis (μ^2/a^3) in combination with eq 3 provides independent, continuum model estimates of λ_S for the nonaromatic, dipolar solvents (eq 3, Table 2).

$$\lambda_S (\text{cont.}) = \frac{\mu^2}{a^3} \left(\frac{\epsilon - 1}{2\epsilon + 1} - \frac{n^2 - 1}{2n^2 + 1} \right) \quad (3)$$

The λ_S values determined by line shape analyses are 0.29–0.37 eV larger than the continuum estimates. A significant part of this discrepancy derives from the vibrational reorganization involving the dimethylamino group (~ 0.17 eV, vide supra). The origin of the residual 0.1–0.2 eV difference is not clear. The other solvents in Table 2 are weakly polar aromatics. Continuum model predictions of λ_S for these solvents are usually too small

(18) CT spectra were obtained from the experimental data by subtracting a scaled acceptor only spectrum and a scaled impurity emission spectrum. The CT Franck Condon line shape was obtained from the CT spectra through division by ν^3 . This accounts for the ν^3 dependence of the Einstein transition probability, the ν^{-2} dependence of the transition moment, and the ν^2 that accompanies conversion from nm to cm⁻¹ units. The energy of the CT Franck–Condon maximum, $h\nu_{\text{FC-max}}$, was determined from a quadratic fit to the top 15% of the Franck–Condon line shape.

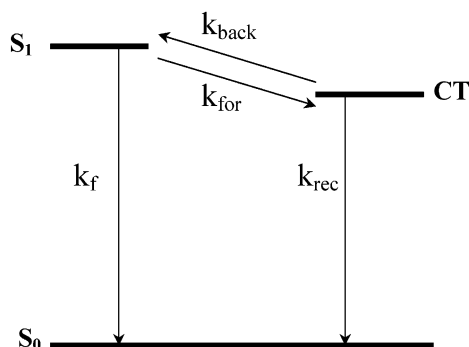
(19) (a) Matyushov, D. V.; Voth, G. A. *J. Chem. Phys.* **1999**, *111*, 3630. (b) Reynolds, L.; Gardecki, J. A.; Frankland, S. J. V.; Hornig, M. L.; Maroncelli, M. *J. Phys. Chem.* **1996**, *100*, 10337. (c) Read, I.; Napper, A.; Zimmt, M. B.; Waldeck, D. H. *J. Phys. Chem. A* **2000**, *104*, 9385.

(20) (a) Matyushov, D. V.; Voth, G. A. *J. Phys. Chem. A* **2000**, *104*, 6485. (b) Vath, P.; Zimmt, M. B.; Matyushov, D. V.; Voth, G. A. *J. Phys. Chem. B* **1999**, *103*, 9130.

(21) NIST Chemistry WebBook, NIST Standard Reference Database Number 69 – March, 2003 Release. <http://webbook.nist.gov/chemistry/>.

(22) (a) Vibrational modes and frequencies determined using the Hartree–Fock method and the 6-31G** basis set^{22b} as implemented in TITAN.^{22c} (b) Hehre, W. J.; Radom, L.; Schleyer, P. v. R.; Pople, J. A. *Ab Initio Molecular Orbital Theory*; Wiley: New York, 1986. (c) TITAN, Wavefunction, Inc., Irvine, CA.

(23) (a) Marcus, R. A.; Sutin, N. *Biochim. Biophys. Acta* **1985**, *811*, 265. (b) Sutin, N. *Acc Chem. Res.* **1982**, *15*, 275.

Scheme 2. Fundamental Rate Processes Following Photoexcitation of **1**

because quadrupolar solvation is not included.¹⁹ One can define “effective” dielectric constants, ϵ_{EFF} , for the aromatic solvents using the Lippert–Mataga slope, the solvent refractive indices, and the CT emission maxima (Table 2). This procedure doubles benzene’s dielectric constant, enhances those of toluene and anisole by 50%, but leaves chlorobenzene’s unchanged. The “continuum” λ_S values calculated using the ϵ_{EFF} for the aromatic solvents (Table 2) are smaller than the line shape values by 0.18–0.38 eV. The underestimates for the aromatic solvents are comparable to those found for the nonaromatic solvents and may be explained similarly.

The CT emission full width at half-maximum is smallest in chlorobenzene. Fitting the CT line shape in this solvent yields the smallest value of λ_S and the lowest CT state energy (Table 2). This contrasts with the continuum estimates of λ_S and the CT state energy for chlorobenzene, which lie roughly in the middle of the ranges predicted for all of the solvents. The small λ_S and low CT state energy translate into a small activation barrier and a large driving force for electron transfer in chlorobenzene. Analysis of the kinetic data using these spectral fitting parameters produces a small value of the electronic coupling in chlorobenzene (vide infra). The origin of the small CT spectral width in chlorobenzene is unknown.

C. Electron-Transfer Rate Constants and Coupling Magnitudes. The shape of the time-resolved fluorescence signal from **1** depends strongly on the detection wavelength, sample temperature, and solvent. If fluorescence is detected at a wavelength where the charge-transfer band dominates, for example, 540 nm, the emission intensity rises and reaches a maximum within a few nanoseconds after excitation. The subsequent decay of the emission intensity requires many hundreds of nanoseconds. By contrast, the fluorescence intensity decays to a small fraction of its peak value within a few nanoseconds following excitation when detecting at 380 nm where pyrene emission dominates. The residual emission intensity requires many hundreds of nanoseconds to decay. Increasing the sample temperature reduces the time required for the fast intensity decay (growth) observed at 380 (540) nm. In toluene and benzene, increasing the sample temperature increases the amplitude of the long-lived component detected at 380 nm. In solvents more polar than benzene or toluene, the amplitude of this long-lived component ($\sim 3\%$) is temperature independent.

The solvent and temperature dependences of the emission decay profile indicate the establishment of an excited-state equilibrium between the pyrene S_1 and CT states of **1** (Scheme

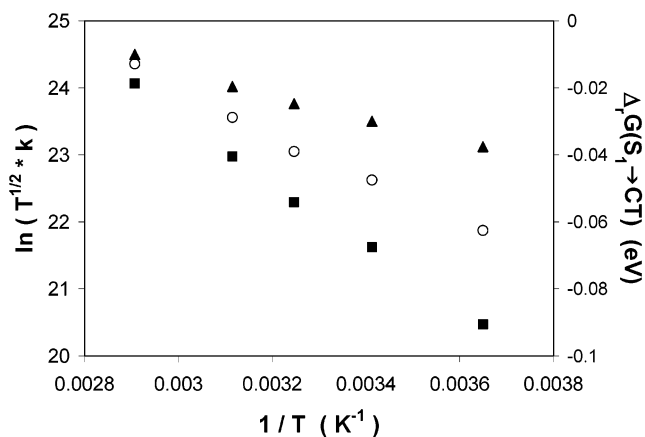


Figure 4. Left axis: Arrhenius type plot of k_{for} (▲) and k_{back} (■) for **1** in toluene versus the reciprocal temperature. Right axis: Plot of $\Delta_r G(S_1 \rightarrow CT)$ (○) versus the reciprocal temperature.

2).²⁴ The initially prepared pyrene S_1 state evolves to an interconverting mixture of S_1 and CT. The equilibrium constant for this step depends on the charge separation driving force, $\Delta_r G(S_1 \rightarrow CT)$ and the sample temperature. Back transfer from CT to S_1 occurs to a measurable extent only if $\Delta_r G(S_1 \rightarrow CT)$ is more positive than -0.12 eV. The equations relating the observed fluorescence decay parameters to the four rate constants in Scheme 2 are well known.⁸ The intrinsic decay rate constants of the pyrene S_1 and CT states (k_f and k_{rec}) are so small that the observed fast decay rate constant is equal to $k_{\text{for}} + k_{\text{back}}$ and the ratio of the fast decay amplitude to the slow decay amplitude detected at 380 nm is equal to $k_{\text{for}}/k_{\text{back}}$. Figure 4 displays the temperature dependence of k_{for} , k_{back} , and $\Delta_r G(S_1 \rightarrow CT)$ determined by analyzing the picosecond photon counting data for **1** in toluene.

The value of $\Delta_r G(S_1 \rightarrow CT)$ determined for **1** from the excited-state equilibrium is -0.05 eV in toluene at 293 K and is -0.11 eV in benzene at 295 K. These two experimental values were used to extract values of ($\hbar\omega$, λ_V , λ_S) from the CT spectra in these two solvents and, ultimately, ($\Delta_r G(CT \rightarrow S_0)$, λ_S) values for the other solvents (vide supra). These reorganization parameters characterize the charge recombination to ground-state reaction, and their use for analyzing the $S_1 \rightarrow CT$ electron-transfer reaction is not rigorously justified. Nevertheless, the CT $\rightarrow S_0$ reorganization parameter sets provide the best estimates for the $S_1 \rightarrow CT$ reaction and will be used in the absence of other information.²⁵

Table 3 lists the charge separation free energy, $\Delta_r G(S_1 \rightarrow CT)$, and charge separation rate constants (k_{for}) determined for

(24) The pyrene–spacer impurity is the source of the long-lived component detected at 380 nm in the solvents more polar than benzene. The absence of a pyrene $S_1 \rightleftharpoons CT$ equilibrium in these solvents was confirmed by the addition of tetrabutylammonium hexafluorophosphate. The salt increased the decay rate constant of the long-lived, CT emission (detected at 520 nm) but did not alter the decay rate constant of the long-lived pyrene emission detected at 380 nm. In benzene and toluene, the long-lived component detected at 380 nm has contributions from both the pyrene–spacer impurity and the pyrene S_1 state in equilibrium with the CT state. The excited-state lifetime of the pyrene–spacer model, **2** (~ 300 ns), and of the CT state of **1** (~ 200 ns, detected at 520 nm) are both longer than the window used to resolve the initial fluorescence decays with picosecond photon counting.

(25) Carter, E. A.; Hynes, J. T. *J. Phys. Chem.* **1989**, *93*, 2184. Carter and Hynes determined that the solvent force constants characterizing fluctuations of a polar solvent about neutral and ion pair states in the same geometry are similar. If the donor–acceptor separations of **1** in the ground, locally excited (S_1) and charge-transfer states (CT) are similar, λ_S should be similar for the $S_1 \rightarrow CT$ and $CT \rightarrow S_0$ reactions.

Table 3. Charge Separation Rate Constants and Electronic Coupling Magnitudes Determined as a Function of Solvent for **1** at 295 K

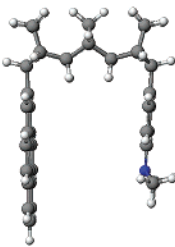
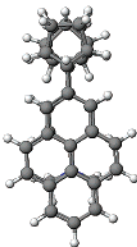
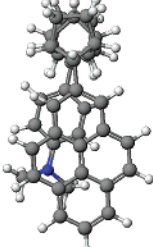
solvent	$I_{\text{P,vert}}$ (eV)	$k(S_1 \rightarrow \text{CT})$ s^{-1}	$\Delta_r G(S_1 \rightarrow \text{CT})$ eV	$ V(S_1 \leftrightarrow \text{CT})^a $ cm^{-1}
anisole	8.4	6.5×10^9	-0.23 ± 0.01	19 ± 1
toluene	8.9	9.4×10^8	-0.05 ± 0.00	23 ± 1
chlorobenzene	9.1	5.6×10^9	-0.30 ± 0.01	7.2 ± 0.5
benzene	9.2	2.2×10^9	-0.11 ± 0.00	19 ± 1
THF	9.6	4.0×10^9	-0.24 ± 0.01	25 ± 3
ethyl ether	9.6	1.4×10^9	-0.09 ± 0.01	27 ± 3
butyl acetate	10.1	1.3×10^9	-0.16 ± 0.01	24 ± 3
ethyl acetate	10.4	1.8×10^9	-0.21 ± 0.01	22 ± 3

^a The reported coupling magnitude is the mean of analyses based on the five ($\hbar\omega$, λ_v , $\Delta_r G(\text{CT} \rightarrow S_0)$, λ_s) parameter sets. The uncertainty reports one standard deviation.

1 at 295 K. The solvents are ordered from smallest to largest vertical ionization potential (column 2). The rate constants vary by less than a factor of 7 from the largest value in anisole to the smallest value in toluene. The small reaction free energy in the latter solvent likely is responsible for the slow transfer rate. Values of the donor–acceptor electronic coupling were determined from the charge separation rate constant⁸ using the single high-frequency mode, semiclassical rate equation²⁶ and the free energy and reorganization parameters determined from the CT spectra. Excluding the chlorobenzene result, the coupling magnitudes exhibit no clear solvent dependence (mean value for seven solvents, $23 \pm 3 \text{ cm}^{-1}$). The values determined for the aromatic solvents are, perhaps, slightly smaller than the values for the nonaromatic solvents, but the difference is comparable to the systematic uncertainties and to the accuracy that this sort of analysis produces. The coupling exhibits no obvious dependence on the solvent ionization potential (HOMO energy) or on the solvent's electron affinity (LUMO energy, data not shown). If solvent mediates donor–acceptor coupling for **1**, its contribution is either minor or weakly solvent dependent.

D. Theoretical Calculations of Electronic Coupling Magnitudes for 1. Because the experimental results indicate that a solvent insensitive pathway is the dominant source of electronic coupling in the charge separation reaction of **1**, through-bond and through-space coupling pathways were evaluated by quantum chemical calculation. The ZINDO²⁷/Generalized Mulliken Hush (GMH)²⁸ method was used to calculate electronic coupling magnitudes between (i) the CT state and the ground state and (ii) the CT state and the S_1 state, which is an equal mixture of the HOMO \rightarrow LUMO+1 and HOMO–1 \rightarrow LUMO configurations. For **1** in its ground-state equilibrium conformation, both calculated couplings magnitudes are at least 1 order of magnitude smaller than the experimental value of the $S_1 \leftrightarrow \text{CT}$ coupling (Scheme 3: Eq. Geom.). Through-bond coupling and direct through-space interaction (6.7 Å) at the equilibrium geometry of **1** do not impart coupling comparable to the experimentally determined values. Consequently, conformational distortions, involving the donor and acceptor groups, were explored to investigate whether higher energy conformations provide larger electronic coupling.

Scheme 3. ZINDO/GMH Calculated Couplings for the Equilibrium and “17° Wag” Conformations

Eq. Geom: Side View	Eq. Geom: End View	17° wag: End View
		
States Coupled	Equilibrium Geometry	17° Wag
$ V (S_0 \leftrightarrow \text{CT})$	1.5 cm^{-1}	6 cm^{-1}
$ V (S_1 \leftrightarrow \text{CT})$	0.6 cm^{-1}	0.5 cm^{-1}

Calculations have been performed for three types of structural deformation. Twisting the spacer such that the donor and acceptor remain in parallel planes but that a 17° dihedral angle is formed by the atoms in the σ bonds connecting these groups to the spacer (Scheme 3: 17° wag) barely alters the $S_1 \leftrightarrow \text{CT}$ coupling, although it increases the $S_0 \leftrightarrow \text{CT}$ coupling 4-fold. Starting from the equilibrium geometry, compression of the donor–acceptor separation by 1.5 Å increases $|V|(S_1 \leftrightarrow \text{CT})$ by only 2 cm^{-1} . In contrast to these ineffectual distortions, rotation of the pyrene about the bond connecting it to the spacer strongly modulates the pyrene/DMA electronic coupling magnitude (Scheme 4). A structure in which the pyrene group is rotated by 45° generates $S_1 \leftrightarrow \text{CT}$ coupling comparable to the experimental values. This rotation positions the edge of the pyrene closer to the dimethylaniline. The source of the coupling increase is discussed below.

Assessing whether twisted pyrene conformations are relevant to the electron-transfer event requires an estimate of their energy and probability of formation. Molecular mechanics calculations indicate that a 22° twist about the bond connecting pyrene to the spacer (the “22° twist” conformer) lies 1.6 kcal/mol above the lowest energy (“0° twist”) conformer and the “45° twist” conformer lies 8.3 kcal/mol above the lowest energy conformer (Scheme 4). Thus, it is feasible that twisting of the aryl groups could be an important nuclear motion for generating electronic coupling.²⁹ Evaluation of the thermally averaged coupling magnitude in a conformationally unconstrained system requires a molecular dynamics/electronic coupling calculation.³⁰ An estimate of the coupling generated by pyrene rotations alone was obtained from the calculated GMH couplings and molecular mechanics energies as a function of the twist angle (Figure 5). The $S_1 \leftrightarrow \text{CT}$ coupling magnitude and the conformer energy vary quadratically with twist angle (between 0° and 45°). Using this dependence on twist angle, a Boltzmann weighted, root-

(26) Kestner, N. R.; Logan, J.; Jortner, J. *J. Phys. Chem.* **1974**, *78*, 2148.

(27) Ridley, J.; Zerner, M. *Theor. Chim. Acta* **1973**, *32*, 111.

(28) (a) Cave, R. J.; Newton, M. D. *Chem. Phys. Lett.* **1996**, *249*, 15. (b) Cave, R. J.; Newton, M. D. *J. Chem. Phys.* **1997**, *106*, 9213.

(29) Semiempirical PM3 calculations place the 22° and 45° twist calculations less than 1 kcal/mol above the lowest energy conformation. Neither the molecular mechanics nor the semiempirical calculation provide the proper Boltzmann weighting for the twisted conformations. However, both calculations demonstrate that twisted conformations are thermally accessible. Use of the PM3 energies yields 13 cm^{-1} as the root-mean-square coupling value at 295 K.

(30) (a) Castner, E. W., Jr.; Kennedy, D.; Cave, R. J. *J. Phys. Chem. A* **2000**, *104*, 2869. (b) Troisi, A.; Ratner, M. D.; Zimmt, M. B. *J. Am. Chem. Soc.*, submitted.

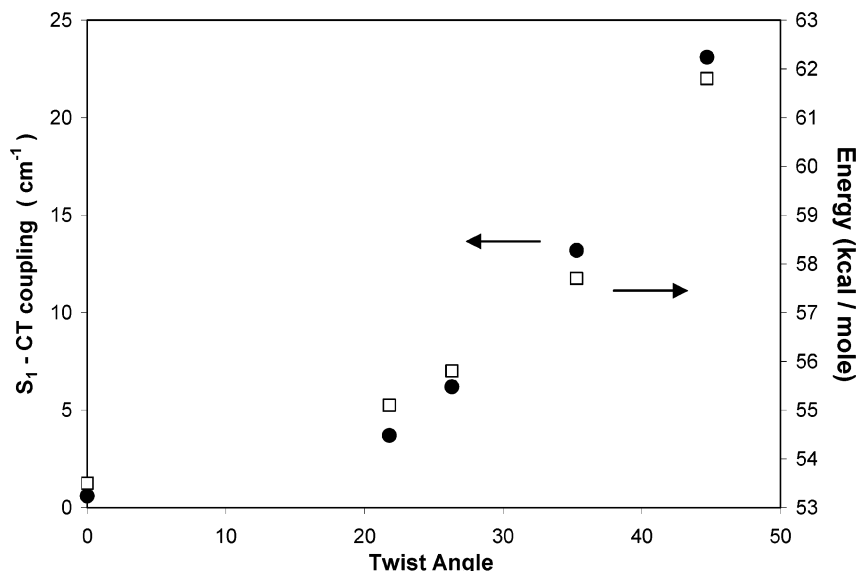
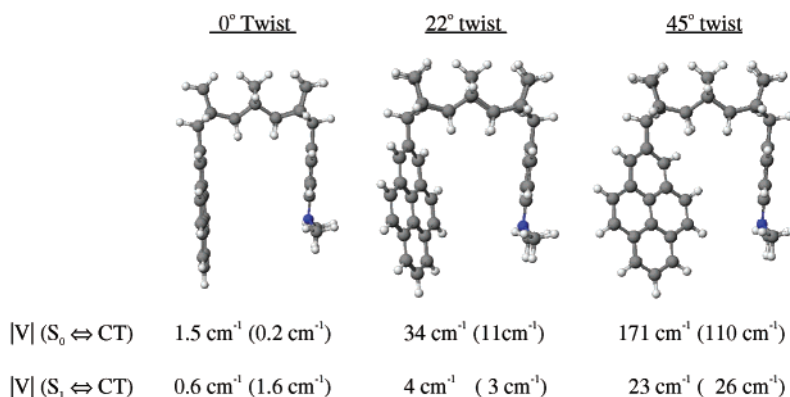


Figure 5. Influence of rotation about the pyrene–spacer bond on the $S_1 \leftrightarrow CT$ electronic coupling (left axis, ●) and the molecular mechanics energy (right axis, □) of molecule **1**. A 0° twist angle corresponds to the lowest energy conformer of molecule **1**.

Scheme 4. ZINDO/GMH Calculated Couplings for the Equilibrium, “ 22° Twist”, and “ 45° Twist” Conformations^a



^a Removal of the central norbornane unit of the spacer generates the couplings listed in parentheses.

mean-square value of the coupling may be calculated⁸ using

$$V_{\text{rms}} = \sqrt{\langle |V|^2 \rangle} = \sqrt{\frac{\sum_j |V_j|^2 \exp(-(E_j - E_0)/kT)}{\sum_j \exp(-(E_j - E_0)/kT)}} \quad (4)$$

where E_j is the energy of a particular conformation, $|V_j|$ is the $S_1 \leftrightarrow CT$ coupling in that conformation, and E_0 is the energy of the most stable conformation. This yields a V_{rms} of 6.6 cm^{-1} at 295 K and 8.4 cm^{-1} at 360 K .²⁹ It is possible that combinations of distortions, for example, pyrene and dimethylaniline rotations and compression, might generate V_{rms} values that approach the experimental values. Interestingly, higher energy conformers of **1** that offer larger $S_1 \leftrightarrow CT$ coupling most likely cannot be populated when solvent molecules are situated in the cleft directly between the donor and acceptor. Thus, solvents that easily enter the cleft might actually reduce the coupling. As both pyrene and dimethylaniline are relatively electron rich, electron-deficient solvents would have the greatest

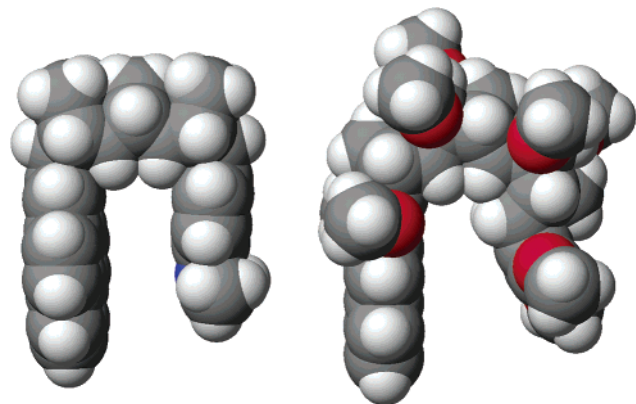
propensity for cleft insertion.³¹ Although the preceding analysis uses a crude molecular mechanics model for the conformer energetics and neglects the energetics of solvent–substrate interactions,³² it illustrates that the conformational freedom of the minimally constrained donor and acceptor groups is a likely source of significant donor–acceptor electronic coupling.

The enhanced coupling attending twisting of the pyrene can be dissected to ascertain whether it arises from changes in through-bond pathways, through-space pathways, or both. ZINDO/GMH values of $|V|(S_1 \leftrightarrow CT)$ are unchanged by removal of the spacer’s central norbornane unit (Scheme 4, values in parentheses) when the donor and acceptor geometries are otherwise maintained as in the full calculation. This finding implicates direct, through-space, donor–acceptor interactions as the primary pathway for $S_1 \leftrightarrow CT$ coupling in the twisted conformers. Through-bond coupling contributions are minimal. This contrasts with the results for $S_0 \leftrightarrow CT$ coupling following clipping of the spacer unit, where through-bond and through-

(31) (a) Klärner, F.-G.; Burkert, U.; Kamieth, M.; Boese, R.; Benet-Buchholz, J. *Chem.-Eur. J.* **1999**, *5*, 1700. (b) Klärner, F.-G.; Panitzky, J.; Blaser, D.; Boese, R. *Tetrahedron* **2001**, *57*, 3673.

(32) Sinnokrot, M. O.; Sherrill, C. D. *J. Phys. Chem.* **2003**, *107*, 8377.

Scheme 5. CPK Models of the Pyrene-Containing, C-Shaped Hole-Transfer Molecule **1** (Left) and the Anthracene-Containing, C-Shaped Electron-Transfer Molecule **3** (Right)



space interactions interfere constructively to generate the coupling. Thus, the S_0 and S_1 states of pyrene in **1** employ different combinations of coupling pathways to interact with the same CT state.

The ZINDO/GMH calculations suggest that the charge separation reactions of **1** obtain $S_1 \rightleftharpoons$ CT coupling from thermally populated, twisted conformers. If this is correct, the electronic coupling in **1** should be temperature dependent.⁸ The charge separation driving force for **1** in benzene at 295 K is the same as for a 7 Å C-shaped molecule, **3**, previously characterized (Scheme 5).⁸ The temperature dependence of $\Delta_r G(S_1 \rightarrow$ CT) in both systems are similar.³³ Despite these similarities, the charge separation rate constants for **1** and **3** exhibit very different temperature dependences: k_{for} in **1** increases with temperature ($E_A \approx 1.8$ kcal/mol), but k_{for} in **3** decreases with temperature ($E_A \approx -1.4$ kcal/mol). The apparent barrier to charge separation is significantly larger for **1** than for **3**. The low-frequency reorganization energy for **1** in benzene is larger than the λ_S attributed to **3** and certainly contributes to the more positive activation energy observed for **1**. A contribution to the larger activation energy from a temperature-dependent electronic coupling in **1** cannot be ruled out, however.

E. Charge Recombination Reactions. Although the $S_1 \rightleftharpoons$ CT electron-transfer kinetics are the primary focus of this investigation, the CT state decay kinetics are noteworthy. The CT state is formed with greater than 98% efficiency, and its decay rate constant, which ranges from 4×10^6 s⁻¹ in tetrahydrofuran to 9×10^6 s⁻¹ in chlorobenzene, is ~ 1000 times smaller than the CT state formation rate constant.³⁴ Numerous processes potentially depopulate the charge-transfer state. Non-radiative CT $\rightarrow S_0$ charge recombination lies deep within the Marcus inverted region: $\Delta_r G(\text{CT} \rightarrow S_0) \approx -3.1$ eV. Using the reorganization parameters obtained from the charge-transfer band line shape fitting, the $|V|(S_0 \rightleftharpoons \text{CT})$ coupling magnitude would need to be larger than 2000 cm⁻¹ to produce the observed decay rate constants. Although couplings of this magnitude are known for contact ion pairs and short donor–bridge–acceptor molecules,³⁵ the calculated GMH couplings are not close to this magnitude. Thus, nonradiative CT $\rightarrow S_0$ transitions are not the dominant CT decay process. The charge-transfer emission

quantum yield is less than 0.05, so radiative CT $\rightarrow S_0$ charge recombination is also not the dominant decay process. Diffusion-controlled, intermolecular charge shift reactions are too slow because the DSA concentration is less than $10 \mu\text{M}$. Other possible contributors to the decay of the CT emission include charge recombination with direct formation of the pyrene triplet³⁶ and a two-step process for formation of the pyrene triplet involving intersystem crossing to the ³CT state followed by charge recombination.³⁷ The pyrene triplet state energy is 2.1 eV; thus CT $\rightarrow T_1$ charge recombination processes lie close to the peak of the Marcus curve in these solvents. Donor–acceptor coupling $|V|(T_1 \rightleftharpoons {}^1,{}^3\text{CT})$ of 1 cm⁻¹ or less is sufficient to produce the observed rate constants using the estimated reorganization parameters. Pyrene triplet is likely the dominant product formed from the CT state.

IV. Conclusion

For the C-shaped pyrene*–spacer–dimethylaniline molecule investigated here, the coupling is essentially solvent independent. No correlation between coupling magnitude and solvent HOMO or LUMO energy is discernible. The shape of molecule **1** in its equilibrium geometry is similar to that of a C-shaped molecule, **3**, previously used extensively in investigations of solvent-mediated electronic coupling (Scheme 5). Two structural differences between these molecules are likely responsible for their disparate sensitivity to solvent-mediated coupling. The donor and acceptor “walls” defining the solvent-accessible cleft in the lowest energy conformation of molecule **1** are parallel to each other and separated by 6.7 Å. The corresponding “walls” in **3** are angled slightly, generating a cleft whose static width varies between 6.9 and 7.4 Å. In both molecules, the thickness of the donor and acceptor excludes ~ 3.5 Å of the cleft. Thus, the wider, wedge-shaped cleft **3** may be more amenable to solvent entry. Mixed solvent NMR studies confirm that benzene entry into the cleft of **1** is not facile.¹¹ The second major structural difference between these molecules is the connection to the spacer. The donor and acceptor in **3** are each “rigidly” attached to the spacer by two σ bonds, so there is only one thermally accessible conformation of the molecule. By contrast, the donor and acceptor in **1** are each attached to the spacer by a single σ bond. The barriers to rotation about these σ bonds are small, and rotation of the donor and acceptor groups sharply reduces the cleft size of **1**, making solvent entry more difficult, and brings the edges of the donor and acceptor into proximity, enhancing the direct through-space electronic interaction. The failure to observe solvent-mediated coupling for **1** likely results from the small separation of the donor and acceptor groups (< 6.7 Å) and because of their conformational freedom.

Although the donor and acceptor group conformational mobility obviates significant solvent-mediated coupling pathways, it allows the donor and acceptor moieties to approach

(33) (a) $(\partial\Delta_r G)/(\partial T) = -1$ meV/K for **3**;^{7c} $(\partial\Delta_r G)/(\partial T) = -1.1$ meV/K for **1**. (34) The CT state decay rate constants for **1** in other solvents are benzene 7.0×10^6 s⁻¹; anisole 7.6×10^6 s⁻¹; BuOAc 7.7×10^6 s⁻¹; ethyl ether 5.6×10^6 s⁻¹.

(35) (a) Gould, I. R.; Young, R. H.; Mueller, L. J.; Albrecht, A. C.; Farid, S. J. *Am. Chem. Soc.* **1994**, *116*, 8188. (b) Pasman, P.; Rob, F.; Verhoeven, J. W. *J. Am. Chem. Soc.* **1982**, *104*, 5127. (c) Oevering, H.; Verhoeven, J. W.; Paddon-Row, M. N.; Warman, J. M. *Tetrahedron* **1989**, *45*, 4751. (36) The dimethylaniline triplet state is slightly higher in energy than the CT state in these solvents. Murov, S. L.; Carmichael, I.; Hug, G. L. *Handbook of Photochemistry*, 2nd ed.; Marcel Dekker: New York, 1993. (37) (a) Liddell, P. A.; Kuciauskas, D.; Sumida, J. P.; Nash, B.; Nguyen, D.; Moore, A. L.; Moore, T. A.; Gust, D. *J. Am. Chem. Soc.* **1997**, *119*, 1400. (b) Roest, M. R.; Oliver, A. M.; Paddon-Row, M. N.; Verhoeven, J. W. *J. Phys. Chem. A* **1997**, *101*, 4867. (c) Lukas, A. S.; Bushard, P. J.; Weiss, E. A.; Wasielewski, M. R. *J. Am. Chem. Soc.* **2003**, *125*, 3921.

near van der Waals contact and enables direct, through-space electronic interaction. This importance of this process was evaluated through a combination of GMH/ZINDO and molecular mechanics calculations. The GMH calculations reveal that twisted pyrene conformers have significant electronic coupling magnitudes. Although only a small sample of **1**'s conformations are explored here, they illustrate the enhanced coupling afforded in some higher energy conformations and suggest that a more extensive theoretical study will demonstrate significant dependence of the electronic coupling on nuclear geometry. Within this model, the experimentally derived electronic couplings reported in Table 3 must correspond to ensemble averages of different donor to acceptor geometries.

Most electron-transfer investigations tacitly assume that any variation of the donor acceptor electron coupling with nuclear structure is unimportant. Both this and prior investigations of electron transfer in C-shaped molecules find coupling variations with nuclear structure to be of considerable importance. The most appropriate framework within which to interpret the dynamics of such systems has yet to be established. One particular case, conformational gating of electron-transfer reactions, has been treated theoretically and analyzed in a number of protein systems.⁴ The dynamics of **1** fall into a different limit and delineate a new direction of investigation. Beratan and Onuchic analyzed the role of nuclear dynamics in determining the adiabatic or nonadiabatic character of an electron-transfer process.³⁸ Their analysis highlighted the importance of two time scales: the characteristic time a system spends in the Landau–Zener (transition state) region, τ_{LZ} , and the time required to interconvert the reactant electronic state to the product electronic state, $\tau_H = \hbar/|V|$. Provided $\tau_{LZ} \ll \tau_H$, a reaction is nonadiabatic. Analysis of the electron-transfer reactions of **1**, using the nonadiabatic approximation, generated $|V| \approx 20 \text{ cm}^{-1}$ so that $\tau_H \approx 10^{-11} \text{ s}$. The polarization relaxation times for the solvents employed here limit τ_{LZ} to time scales of 10^{-12} – 10^{-13} s or less. Comparison of these time scales indicates that the electron-transfer reactions of **1** lie in the nonadiabatic regime. However, the electron-transfer process for **1** is coupled to torsional (and other) motions of the donor and acceptor units. Given a torsional

frequency of $6 \times 10^{11} \text{ Hz}$,³⁹ we estimate a 1 ps correlation time, τ_v , for fluctuations of the electronic coupling due to the nuclear motions of **1**. Hence, the three relevant time scales are ordered $\tau_{LZ} \leq \tau_v < \tau_H$, and the following picture of the dynamics for **1** is proposed.

During any single entry into the transition state region, the electronic coupling is relatively constant and the transition probability is small. Thus, the transfer event should remain nonadiabatic. However, each time the transition state region is accessed, the value of the coupling is different due to its strong dependence on nuclear structure. As a result, the experimentally determined coupling value is a root-mean-square average (eq 4) over the thermally accessible conformations. In this limit, the dependence of the electronic coupling on the nuclear coordinate is not immediately obvious in the kinetics. It should be possible to reveal the nuclear coordinate dependence of the coupling by modifying the relative ordering of the three time scales. For example, a significant increase of τ_v , such that $\tau_v \gg \tau_H > \tau_{LZ}$, would produce a distribution of persistent coupling magnitudes and generate a range of transfer rate constants.⁵¹ The fluorescence decay kinetics in such a system would appear nonexponential.

The role of nuclear dynamics in accessing the electron-transfer transition state is well understood. By contrast, the implications of the electronic coupling itself being coupled to nuclear dynamics are not well established. Future studies, in which the conformational motion is inhibited, should allow exploration of an electron-transfer mechanism that is controlled by the torsional motion of the donor and acceptor groups and investigation of the dynamics in the regime $\tau_v/\tau_H \approx 1$ to $\tau_v/\tau_H \gg 1$.

Acknowledgment. We thank the National Science Foundation (CHE-0108945 to M.B.Z. and CHE-0111435 to D.H.W.), Professor V. Fidler (Prague) for enlightening discussions, Dr. Andrew Napper for invaluable assistance with the SPC experiments, and Dr. M. Newton for assistance with GMH calculations.

JA0372917

(38) (a) Onuchic, J. N.; Beratan, D. N.; Hopfield, J. J. *J. Phys. Chem.* **1986**, *90*, 3707. (b) Sumi, H.; Marcus, R. A. *J. Chem. Phys.* **1986**, *84*, 4894.

(39) The moment of inertia about the pyrene long axis is $498 \text{ amu } \text{Å}^2$. The curvature, C , according to molecular mechanics is $7.21 \times 10^4 \text{ J/(mol rad}^2)$. The frequency of the pyrene oscillation about its long axis is $\omega = (2C/I)^{1/2} = 3.8 \times 10^{12} \text{ rad/s} = 6 \times 10^{11} \text{ Hz}$.